



Fractional damping enhances chaos in the nonlinear Helmholtz oscillator

Adolfo Ortiz · Jianhua Yang ·
Mattia Coccolo  · Jesús M. Seoane ·
Miguel A. F. Sanjuán

Received: 30 July 2020 / Accepted: 2 November 2020
© Springer Nature B.V. 2020

Abstract The main purpose of this paper is to study both the underdamped and the overdamped dynamics of the nonlinear Helmholtz oscillator with a fractional-order damping. For that purpose, we use the Grünwald–Letnikov fractional derivative algorithm in order to get the numerical simulations. Here, we investigate the effect of taking the fractional derivative in the dissipative term in function of the parameter α . Our main findings show that the trajectories can remain inside the well or can escape from it depending on α which plays the role of a control parameter. Besides, the parameter α is also relevant for the creation or destruction of chaotic motions. On the other hand, the study of the escape times of the particles from the well, as a result of variations of the initial conditions and the under-going force F , is reported by the use of visualization techniques such as basins of attraction and bifurcation diagrams, showing a good agreement with previous

results. Finally, the study of the escape times versus the fractional parameter α shows an exponential decay which goes to zero when α is larger than one. All the results have been carried out for weak damping where chaotic motions can take place in the non-fractional case and also for a stronger damping (overdamped case), where the influence of the fractional term plays a crucial role to enhance chaotic motions. We expect that these results can be of interest in the field of fractional calculus and its applications.

Keywords Nonlinear oscillations · Delay systems · Resonance · Fractional derivatives

1 Introduction

Fractional calculus is an area of the mathematical analysis. It studies the possibilities of taking real or even complex numbers as orders of the integral and derivatives on a known or unknown function. Such operators are rather useful in science and engineering. Also, fractional differential operators involve defined integrals over a time domain, and this poses significant memory effects as shown in Ref. [1]. For these reasons, the fractional calculus has gained much attention and relevance in the past few years due to its applications to several research fields such as control systems, nonlinear oscillators, potential fields, diffusion problems, viscoelasticity and rheology, synchronization, thermodynamics, biology among others [2–9]. In the case of

A. Ortiz
Centro de Investigación en Micro y Nanotecnología,
Facultad de Ingeniería, Universidad Veracruzana, Calz.
Ruiz Cortinez 455, CP 94294 Boca del Río, Veracruz,
México

J. Yang
School of Mechatronic Engineering, China University of
Mining and Technology, Xuzhou 221116, People's
Republic of China

M. Coccolo (✉) · J. M. Seoane · M. A. F. Sanjuán
Nonlinear Dynamics, Chaos and Complex Systems Group,
Departamento de Física, Universidad Rey Juan Carlos,
Tulipán s/n, Móstoles, 28933 Madrid, Spain
e-mail: mattiatommaso.coccolo@urjc.es

nonlinear oscillators, the research has been very extensive with interesting results, especially in the study of the effect of introducing a fractional derivative in the damping term [10]. In the last reference, the Authors carried out the study of chaos detection in the Duffing oscillator by using the Melnikov Method. On the other hand, the detection of chaos in fractional systems by using SALI has been developed in Ref. [11]. Furthermore, the fractional Duffing equation in the presence of nonharmonic external perturbations has been also studied with detail in Ref. [12]. Recent and very complete reviews on the current research and real applications of fractional calculus in science and engineering can be found in Refs. [13–18].

In our present work, due to the fact that the dissipation plays an important role in the evolution of the systems, we focus our interest in analyzing the effect of a fractional damping on a nonlinear oscillator dynamics. In fact, we modify the equation of motion of the Helmholtz oscillator, which is being used in many physical problems, in order to introduce a fractional differential operator in the damping term instead of the classical derivatives. Then, we focus our attention on the effect of the fractional operator on the dynamics of the system by studying the behavior of the trajectories, this means, if the asymptotic solutions fall inside or outside the potential well defined by the Helmholtz potential. This is analyzed using the *Grünwald–Letnikov* fractional derivative algorithm [1, 19] for our numerical simulations, in which we change certain initial condition, the fractional derivative and the forcing amplitude for two values of the damping parameter. These two damping values have been chosen in order to set the system in an underdamped or in an overdamped case.

In fact, the Helmholtz oscillator has a very rich dynamical behavior for small values of the damping parameter where both, chaotic and periodic motions can take place and also escapes from the potential well are possible. On the other hand, when the damping parameter grows, the system becomes more and more predictable until all particles fall into the well. However, in the overdamped case, the effect of the fractional derivative can generate different kind of motions, including chaotic motion. That is why the underdamped case has been the most interesting one to study in the nonlinear dynamics field in the last decades, but the overdamped case can be interesting when fractional derivatives are involved.

By using the above algorithm, we calculate the orbits in phase space and show, in the parameter space, the attractor and the escape times, i.e., the final state of the trajectories, inside or outside the potential well, and the time to reach such state, respectively. The parameters that we change in the simulations are the damping term μ , the fractional derivative α , the forcing F and the initial condition x_0 . For visualization purposes, we have plotted in parameter space, both the attractor and the escape time gradient (as can be seen along the manuscript). In these figures, it is possible to appreciate the complexity of the relation between the fractional parameter and the dynamics of the system. In fact, the attractor boundaries show some sort of fractalization, which means that a small deviation in the parameters value can lead to drastically different solutions, i.e., the system asymptotic behavior can stay inside the well or leave it. It clearly means that in the fractal regions, errors in the parameters might cause different final states as is well-known in chaotic systems. Indeed, these results show that using the fractional parameter α as a control parameter can provide different dynamics for the dynamical system, either periodic or chaotic motions and transitions between them. This is precisely one of the main goals of the research work reported here by using phase-space visualizations techniques. Among the goals, we can find a natural extension to the fractional case the well-known results obtained for the non-fractional case in both cases, the underdamped and the overdamped regimes.

The organization of this paper is as follows. We describe the fractional damped Helmholtz oscillator, in Sect. 2. The dependence of the trajectories in function of the fractional parameter α for the underdamped case is carried out in Sect. 3. Section 4 shows the distribution of the escape times of the particles from the potential well versus α and also the analysis of the bifurcation diagrams in function of α for an overdamped case. Conclusions and a discussion of the main results of this paper are presented in Sect. 5.

2 Fractional damped Helmholtz oscillator

The Helmholtz oscillator is represented by a nonlinear second order differential equation considering the presence of the potential defined as $V(x) = \frac{1}{2}x^2 - \frac{1}{3}x^3$, as shown in Fig. 1. It represents the equation of motion of a unit mass particle in this potential under the influence

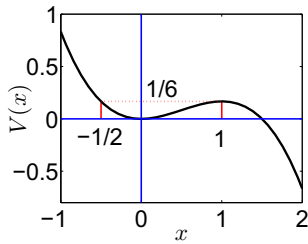


Fig. 1 Plot of the potential well defined through the function $V(x) = \frac{1}{2}x^2 - \frac{1}{3}x^3$. Note that for the interval $x \in [-\frac{1}{2}, 1]$ in absence of forcing and friction the orbits are bounded

of both a periodic forcing and a dissipative force and is given by

$$\ddot{x} + \mu\dot{x} + x - x^2 = F \cos(\omega t), \tag{1}$$

where μ is the damping parameter, F and ω the forcing amplitude, and the forcing frequency, respectively, taking all of them positive values. Normally, the damping term, considered like the first derivative in Eq. (1), has an impact proportional to the constant μ in the system. In what follows, the first derivative of Eq. (1) is replaced by an order α fractional derivative, i.e., $\dot{x}(t) \rightarrow D^\alpha x(t)$, for which we have the *Fractional Helmholtz Oscillator*. We consider this exchange because of the interest in looking for a more general dynamics of the oscillator as a consequence of considering the memory effects through the fractional operator. As a matter of fact, the most relevant objective here is to investigate changes over the whole dynamics taking fractional order derivatives in the interval $[0, 2]$ of α values, as is usually studied in the context of fractional nonlinear oscillators. Then, the *fractional Helmholtz oscillator* with fractional damping reads

$$\ddot{x} + \mu D^\alpha x + x - x^2 = F \cos(\omega t), \tag{2}$$

with the additive property of the fractional derivative, one can get a new system for the purpose of our numerical simulations, which can be expressed as:

$$D^{\alpha_1} D^{\alpha_2} x(t) = D^{\alpha_1 + \alpha_2} x(t) \tag{3}$$

Thus, the new system is composed by a set of three fractional differential equations according to Eq. (3) and they read as follows:

$$\begin{aligned} D^\alpha x &= y \\ D^{1-\alpha} y &= z \\ Dz &= F \cos(\omega t) + x^2 - x - \mu y, \end{aligned} \tag{4}$$

where z is a mathematical component coming from the transformation of the model into a fractional order

system. To perform the solution of Eqs. (4), we use the *Grünwald–Letnikov* [19] fractional derivative, for which the algorithm to numerically solve this system is given by

$$\begin{aligned} x(t_k) &= y(t_{k-1})h^\alpha - \sum_{j=v}^k c_j^{(\alpha)} x(t_{k-j}) \\ y(t_k) &= z(t_{k-1})h^{1-\alpha} - \sum_{j=v}^k c_j^{(1-\alpha)} y(t_{k-j}) \\ z(t_k) &= \Psi h - \sum_{j=v}^k c_j^{(1)} z(t_{k-j}), \end{aligned} \tag{5}$$

where $\Psi = F \cos(\omega t_k) + x^2(t_k) - x(t_k) - \mu y(t_k)$ and h is the discrete time step. The coefficients c_j^α are the binomial coefficients derived in the numerical scheme implemented, $c_0^\alpha = 1$ and

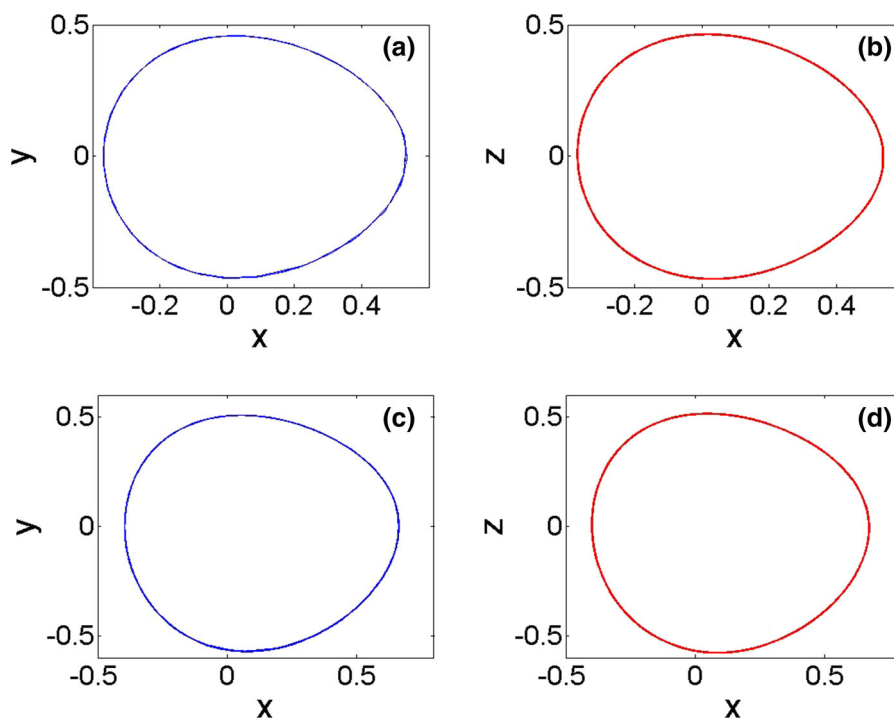
$$c_j^\alpha = \left(1 - \frac{\alpha + 1}{j}\right) c_{j-1}^\alpha. \tag{6}$$

In the next subsection, we numerically analyze the dynamics of our model with the fractional algorithm for $\alpha = 1$ and with a non-fractional algorithm. Then, we compare the results.

In order, and with the only purpose, to test the numerical solutions of the fractional numerical scheme, a comparison with a fourth-order Runge–Kutta method is carried out. This comparison only is possible for $\mu = 0$ or $\alpha = 1$ which corresponds with the non-fractional case.

In Fig. 2, we show the resulting orbits starting at zero initial conditions, which means $(x_0, y_0, z_0) = (0, 0, 0)$, for both cases the underdamped and the overdamped, the other parameter values are shown in the caption. In Fig. 2a–c, the trajectories are calculated by using the Runge–Kutta method, and in Figs. 2b–d with the Grünwald–Letnikov method with $\alpha = 1$. In this case, the fractional method scheme gives us the same trajectories as the one for the Runge–Kutta method, showing bounded motions of the particle inside the potential well. This is a first proof of the adequate response of the fractional algorithm. Now, we focus on an interesting point that we investigate, the existence of orbits that escape from the potential well, defined above, and the time that the particles need to leave the potential well, namely the escape time. In Fig. 3, we represent an extra comparison between the two methods by plotting the escape times of the orbits varying

Fig. 2 Comparison between solutions provided by distinct methods for the damped Helmholtz oscillator at the zero initial conditions with $\mu = 0.1$ and $F = 0.1$ in panels (a) and (b), $\mu = 0.8$ and $F = 0.46$ in panels (c) and (d). Panels a and c show the trajectories of the solution of the fourth-order Runge–Kutta scheme. Panels b and d show the trajectories of the solution of the fractional numerical scheme with $\alpha = 1$



the initial conditions inside the well, for parameter values for which the particles escape from the well. For that purpose, we set $F = 0.46$ and $\omega = 1$ with $\mu = 0.1$ in Fig. 3a–b and with $\mu = 0.8$ in Fig. 3c–d. Then, we vary the initial conditions in the interval $x \in (0.85, 1)$. In the non-fractional Helmholtz oscillator, the effects of dissipation help to keep the particles inside the well. For that reason, when the damping term grows bigger and the system is in an overdamped regime, the dynamics of the system becomes more predictable since for all initial conditions the particles need more time to escape the well and more initial conditions fall into the bottom of the potential well. On the other hand, in the case of weak dissipation, the dynamics of the system are very rich and the escape times become smaller. In fact, in the panel it is possible to appreciate that the escape time follow that trend, since for $\mu = 0.8$ the particle needs more time to leave the potential well. As a summary of our comparison, also here, in the left figures of the panel we have used the Runge–Kutta integrator, while for the others the fractional numerical scheme. In general, the orbits take more time to escape in the fractional scheme, as supported by Fig. 3, due to the characteristics of the Grünwald–Letnikov method of integration [20]. However, for the sake of the results of this paper, we want to stress out that, in both numerical schemes,

the escape time curves follow the same trend. This last affirmation can be proved through the comparison of the fitting curves that appear in the textboxes of each figure. Starting from Fig. 3a–b, we can see that the fitting curve is exponential for both algorithms, but also that the parameter values of the first one falls within the 95% confidence bounds, that are the numbers inside the parenthesis of the other one, and vice versa. The same thing happens for the fitting curves in Fig. 3c–d. Therefore, we can confidently affirm that in both cases, the fitting curves of the escape times calculated with the Runge–Kutta method follow the same equation of the ones calculated with the Grünwald–Letnikov algorithm, and their parameter matches with a confidence at least of the 95%. This gives us another good proof of the reliability of the fractional algorithm. That settled, we can start our analysis of the system.

3 Dynamics of the fractional Helmholtz oscillator in the underdamped case

Here, we show numerical simulations in order to understand the dynamics of the fractional Helmholtz oscillator involving a fractional-order damping for different values of the damping parameter μ . We fix the parameters of the system for the underdamped case

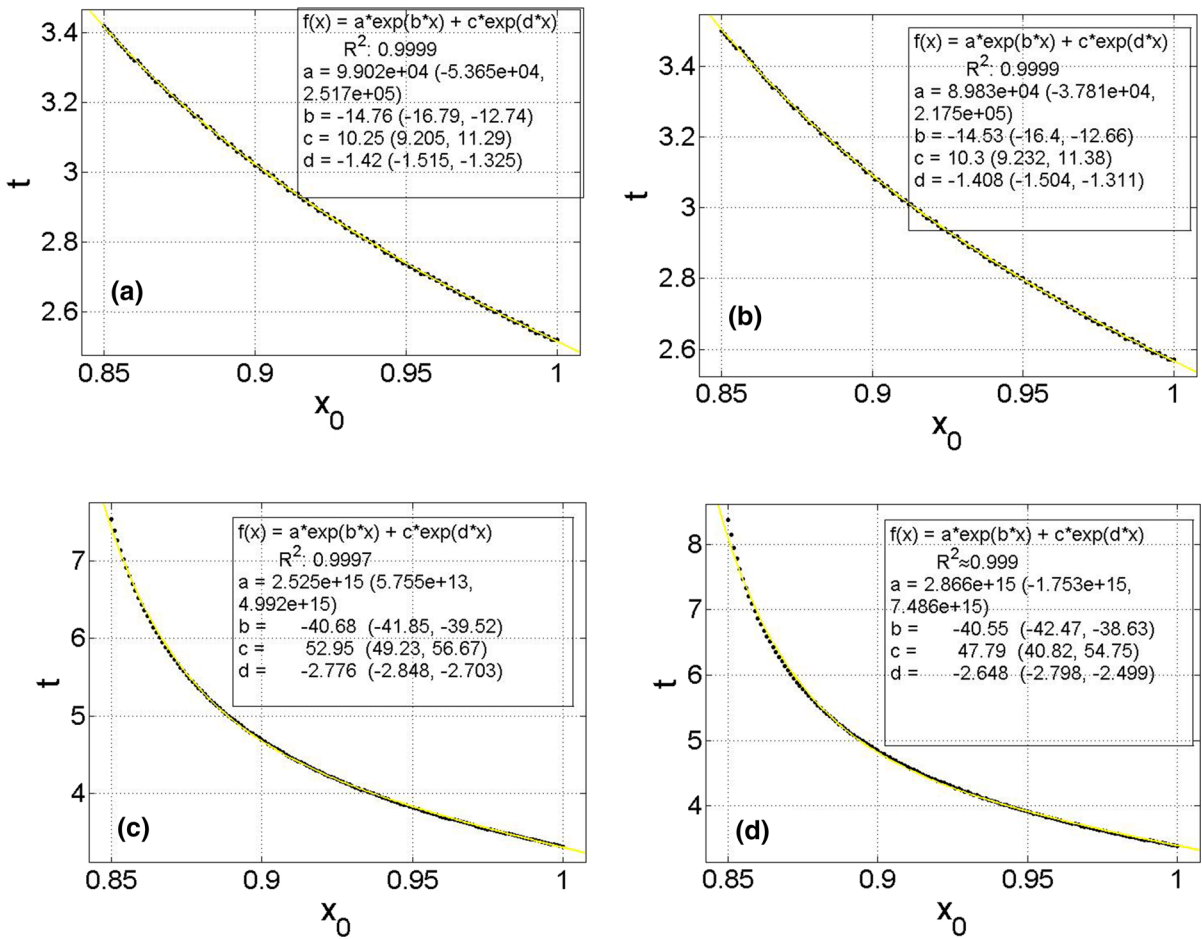


Fig. 3 Comparison between escape times of solutions provided by distinct methods for the damped Helmholtz oscillator at $x_0 \in (0.85, 1)$ with $\mu = 0.1$ in panels (a) and (b), $\mu = 0.8$ in panels (c) and (d). In all the panels, $F = 0.46$ and $\omega = 1$. Panels a and c show the escape times calculated with the Runge–Kutta method. Panels b and d show the escape times calculated with the

fractional numerical scheme and $\alpha = 1$. In the textboxes, we can see the fitting equations and their parameter. Near the parameter, in the parenthesis, we show the 95% confidence bounds. This is important to check that the fitting equations and their parameter values of each couple of panels, (a–b) and (c–d), are compatible within each other

as $\mu = 0.1$, $F = 0.1$ and $\omega = 1$ which are a very convenient choice for this study. In this physical situation, as previously mentioned, the dynamics of the non-fractional Helmholtz oscillator is very rich. In this case, the fractional damping term will add more complexity in both the dynamics and the topology of the system as we show now.

At first, we focus our attention to the final state of the system, whether the trajectories stay inside the potential or leave it. Then, we study the variation of the escape times of the particles from the well. The escape time, t , is the time that the particle spends inside the well before crossing the boundary ($x = 1$ in this model) escaping from it. In fact, we consider that the particle

has escaped when it crosses the point $x > 1$ with a positive velocity, $\dot{x} > 0$. For that purpose, we start with the analysis of the fractional dynamics by changing the α and the x_0 initial condition values and find critical values where the behavior of the system changes abruptly. This analysis keep the other initial condition equal to zero and the same values of the rest of the constant parameters as previously stated.

Thus, Fig. 4a shows the final state of the system by varying the values of the fractional derivative α and the initial condition x_0 . That means that we have plotted the attractors, being an attractor a set of numerical values toward which a system tends to evolve, for a wide variety of starting conditions of the system. So that, it

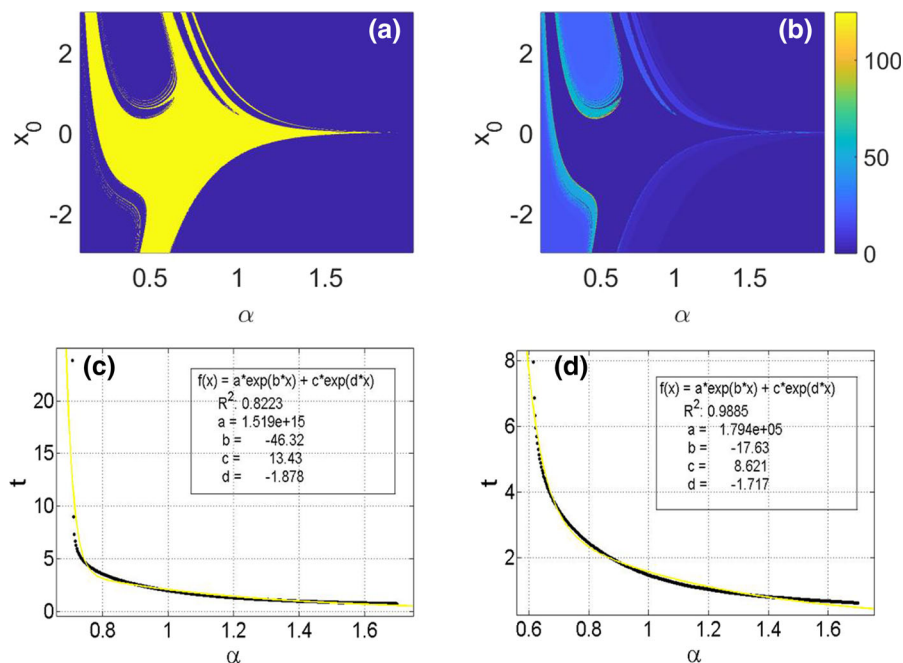


Fig. 4 **a** shows the final state of the system depending on the value of α , from 0.1 to 2, and the variation of the first initial condition x_0 from -3 to 3 . White color (yellow on line) implies that the particle remains inside the well and black color (blue on line) that particle escapes. In **a**, it is possible to see the areas where the boundaries show the fractalization. **b** shows the gradient of

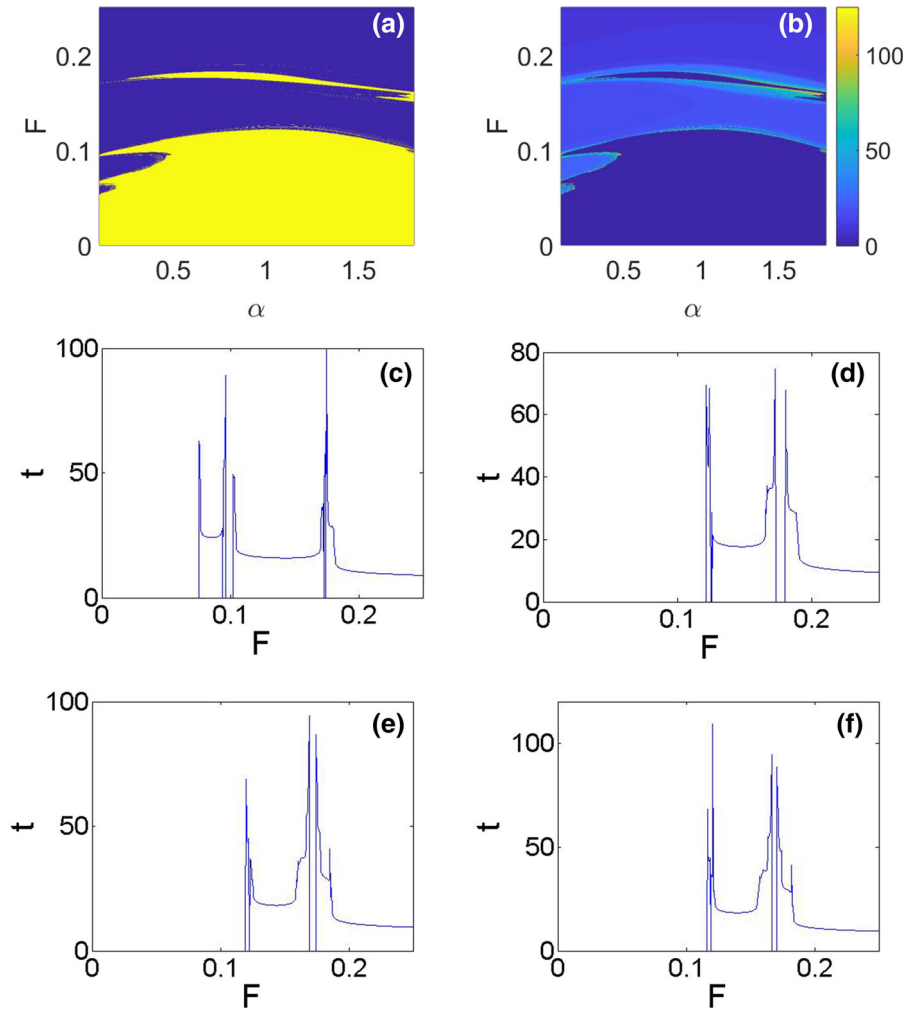
is possible to appreciate two recognizable attractors, the gray one (yellow online) that represent the case when the particle remains inside the well and black one (blue online) that represent when the particles escape. It is, also, possible to appreciate the fractalization of the boundaries between the different region of the figure. In Fig. 4b, we show the gradient of the escape time. Here, it is possible to appreciate that near the boundaries that separate the two attractors defined in Fig. 4a, the escape times are larger and, in particular, in the zones that show fractalization. Also, we depicted the trend of the escape times in function of α to visualize how they change along the boundaries of the attractor. In order to avoid fluctuations in the escape times, we decided to move along the smoother boundary of the attractor, i.e., for $x_0 < 0$ and $\alpha > 0.5$, so we have fixed the initial conditions, $x_0 = -2$, Fig. 4c, and $x_0 = -3$, Fig. 4d and varied α . It is possible to see that the two curves do not share the same trend, as in the first one the exponential curve does not fit the data very well, $R^2 \approx 0.8$, while in the second case, it works perfectly, $R^2 \approx 0.99$. The same thing happens for a fixed α and

the particle escape times from the potential well depending on the α -value and the variation of the first initial condition for the same values of figure (a). **c** and **d** show an example of the trend of the escape time in function of α , for different initial conditions, $x_0 = -2$ and $x_0 = -3$ respectively

varying x_0 . So, we can say that for this value of μ , the trend of the escape times depends on the parameter values, chosen on the boundaries of the attractor. Therefore, it is not possible to find a common decay law for the escape times, just that the farther from the attractor the lower the escape time.

Then, to extend our study of the behavior of the system, we have also decided to plot the final state and the escape time gradient in function of the variation of the α value and the amplitude of the forcing F , for the zero-initial condition, plotted in Fig. 5a–b, respectively. It is interesting to see that for $\alpha = 1$, the particle escapes the potential well for, approximately, all the forcing amplitude values bigger than $F \approx 0.2$, a well-known result [21]. Moreover, it is interesting to stress out that $F \approx 0.2$ seems to be the maximum value of the forcing amplitude for which we can have bounded trajectories independently of the values of α . Also, some details in the figures are interesting, such as the escape region delimited by $0 < \alpha < 0.5$ and by $0.05 < F < 0.1$ and the gap between $F \approx 0.1$ and $F \approx 0.17$, for all the values of α . Also in this case, as in Fig. 4, the higher

Fig. 5 **a** Shows the final state of the system taking $\alpha = [0.1, 1.8]$ and $F = [0, 0.3]$ and keeping constant the rest of the parameters. Gray color (yellow on line) implies the particle that remains inside the potential well and black color (blue on line) that particle escapes from it. **b** shows, for the same range of F and α and the same parameter as in figure (a), the gradient escape times. The other figures show slices of the figure (b), for different α values, such as 0.25, 1, 1.25, 1.39, respectively



escape times are related with the fractalization of the boundaries between the different basins of attraction. In order to have a better insight of Fig. 5b, we have plotted Fig. 5 c–f. These figures have been computed for the zero-initial conditions and different values of the fractional parameter, $\alpha = 0.25$, $\alpha = 1$, $\alpha = 1.25$ and $\alpha = 1.39$, respectively. Here again, it is not possible to establish a trend of the escape time in function of F for a fixed α value, neither it is possible in function of α for a fixed F value, due to the fractalization of the boundaries and the shape of the basins.

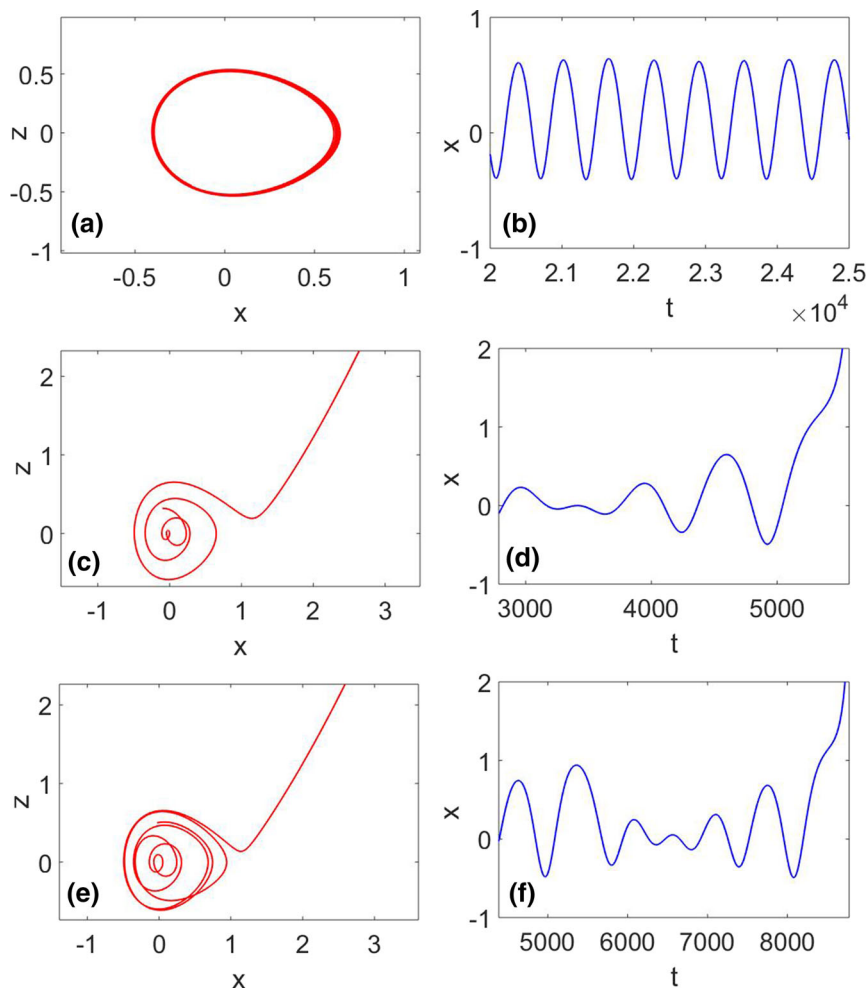
To complete our investigation, we have plotted the Fig. 6. Here, we can find three trajectories in the $x - z$ plane and the time series of $x(t)$. In Fig. 6a–b, we represent a bounded trajectory with its related time series. In Fig. 6c–d, we represent an escaping trajectory and its related time series. In Fig. 6e–f, also an escaping

trajectory and its time series with a larger escape time. This last trajectory has been chosen in a fractal boundary where the escape time are, in effect, larger. In the plot of these last figures, we have chosen the parameter values reported in the captions of the panel by using the data extrapolated by the precedent figures, Figs. 4 and 5, to help visualize the dynamics of the system while the parameters, α , F , x_0 change and the μ parameter is fixed.

4 Dynamics of the fractional Helmholtz oscillator in the overdamped case

In this section, we investigate the effect of large values of the damping parameter μ on the dynamics of the system. So that, now, we study the case with a big-

Fig. 6 Behavior of the fractional damping Helmholtz oscillator with $\mu = 0.1$, $F = 0.1$ and $\omega = 1$. The figures represent the trajectories of the Helmholtz oscillator z vs x and the oscillations of the position x in time with different α values at different initial conditions x_0 . In particular, $\alpha = 0.39$, $x_0 = 0.4$ (a) and (b), $\alpha = 0.4$, $x_0 = 0.4$ (c) and (d), $\alpha = 0.41$, $x_0 = 0.5$ (e) and (f). a and b plots represent the typical bounded orbit inside the potential well. c and d plots show a faster escaping trajectory. e and f plots represent a slower escaping trajectory



ger damping value, $\mu = 0.8$, the overdamped case, of the fractional Helmholtz oscillator. Notice that, as already discussed, in the non-fractional case, the overdamped situation has not physical interest since almost all particles with initial condition inside the well are trapped into the potential well. For that reason, the role of the fractional parameter α will be crucial to enhance chaotic or regular motions and also escapes from the potential well.

For the reader's convenience, we decide to follow the same path as in the previous case and started to plot the final state of the system and the escape times gradient for the simultaneous variation of α and the first initial conditions x_0 , maintaining fixed the value of the amplitude of the forcing $F = 0.46$ and its frequency $\omega = 1$. Notice that with respect to the underdamped case, while the frequency does not change, the forc-

ing amplitude that we use is bigger. The results of the computational experiments are shown in Figs. 7a–c and 8a–c. The first panel shows the final state of the system with the purpose to know whether the particle remains inside the well or escapes from it. Gray color (yellow online) has been used to represent the case when the particle remains inside the well and black color (blue on line) when it escapes. It is possible to appreciate the fractalization of the basins in Fig. 7b–c. In particular, in the second one, we can see that the fractalization starts for $\alpha \approx 1.36$.

Then, Fig. 8a–c shows the gradient of the escape time. Here, it is possible to appreciate that as in the previous case, near the boundaries defining the non-escaping and escaping regions, the escape times are larger and in particular, in the zones that show fractalization.

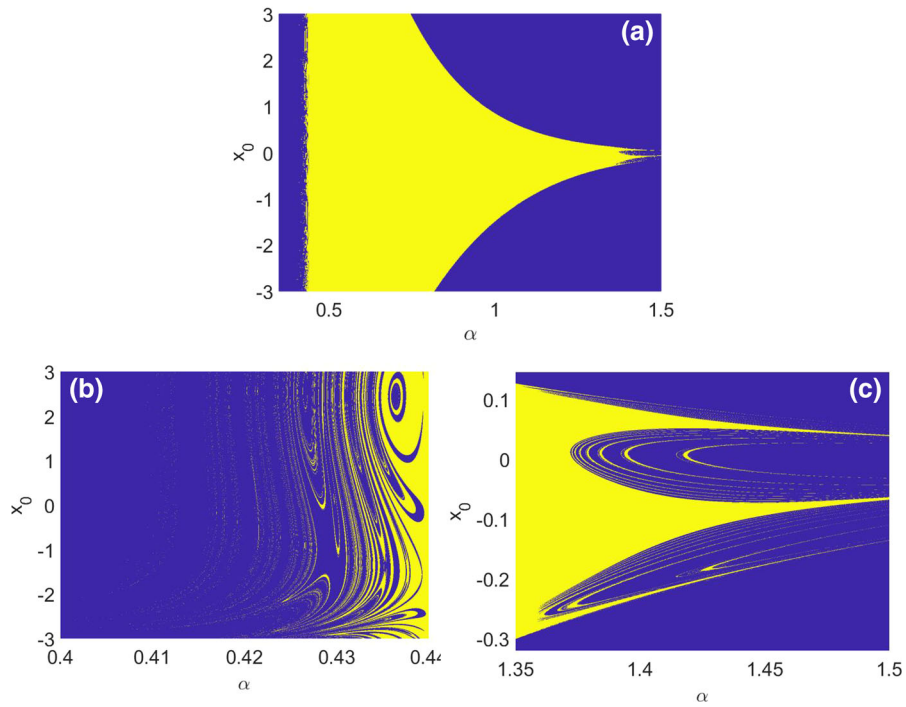
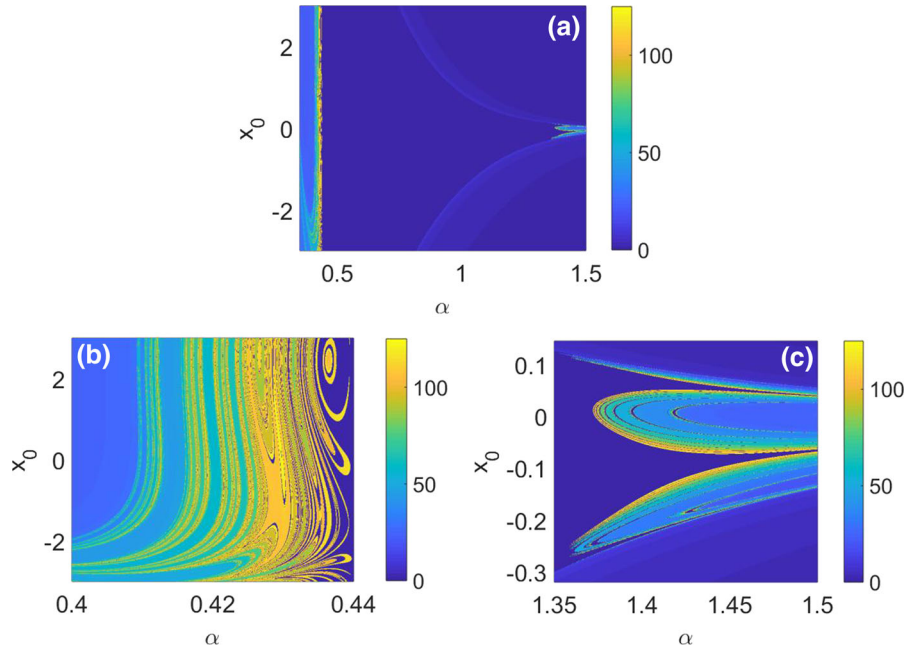


Fig. 7 Final state of the system depending on the α -value and the variation of the first initial condition x_0 from -3 to 3 . White color (yellow on line) implies the particle remains inside the well and black color (blue on line) that particle escapes. **a** We can see in this figure a defined area representing the last state of the particle as time goes on depending on the initial position x_0 and on

the α variation, keeping constant the rest of the parameters of the model. **b** and **c** it is possible to appreciate the zoom of the figure **(a)** for values of $\alpha = (0.4, 0.44)$ and $\alpha = (1.35, 1.5)$, respectively. These last ones are the areas where the boundaries show the fractalization

Fig. 8 **a** shows the gradient of the particle escape times from the potential well depending on the variation of the α value and of the first initial condition x_0 from -3 to 3 . **b** and **c** present a zoom of the most interesting areas of figure **(a)**, i.e., values of $\alpha = (0.4, 0.44)$ and $\alpha = (1.35, 1.5)$, respectively. As stated in the previous panel, the areas where the boundaries show the fractalization



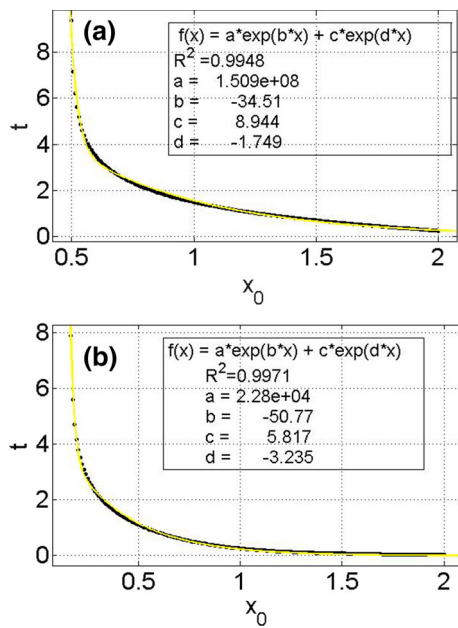


Fig. 9 **a** Average escape times from the well for $\alpha = 1.1$ versus different initial conditions inside the well. **b** Represents the same for $\alpha = 1.3$. It is possible to observe the exponential decay law

In Fig. 9a–b, the escape time of the particle is shown for fixed α and different initial condition x_0 . In Fig. 9, we have set the value of α smaller than $\alpha \approx 1.36$, for which value we previously have found where the fractalization of the attractor boundaries begins, as shown in Fig 7c. So that, as in the underdamped case, we use the existence of smooth boundaries and focus our study on finding a general decay law for the escape time in function of the variation of the initial condition x_0 and the α parameter. Thus, we analyze the effects of the higher damping coefficient on the escape time near the attractor boundaries. We started, in Fig. 9a, b, by varying the initial conditions and fixing the α parameter at $\alpha = 1.1$ and $\alpha = 1.3$, respectively. It is possible to appreciate in both figures the exponential decay law for the time escape in function of the initial condition x_0 where the best fitting is $t(x_0) = ae^{bx_0} + ce^{dx_0}$. For that reason, we have decided to explore the variation of the exponential parameters in the decay law in function of the α parameter.

First of all, we found for $\alpha = 1.36$, some fluctuations in the escape time before the monotonic exponential decay, as shown in Fig. 10. In this last panel, we show the change in the behavior of the escape time of the system, when the α value passes from 1.35 (Fig. 10a)

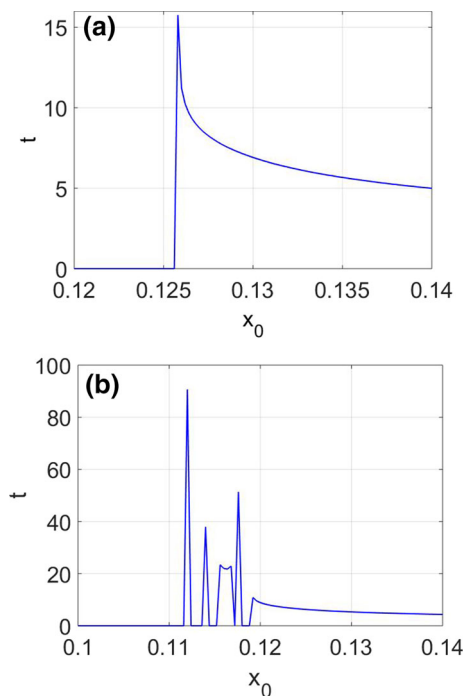
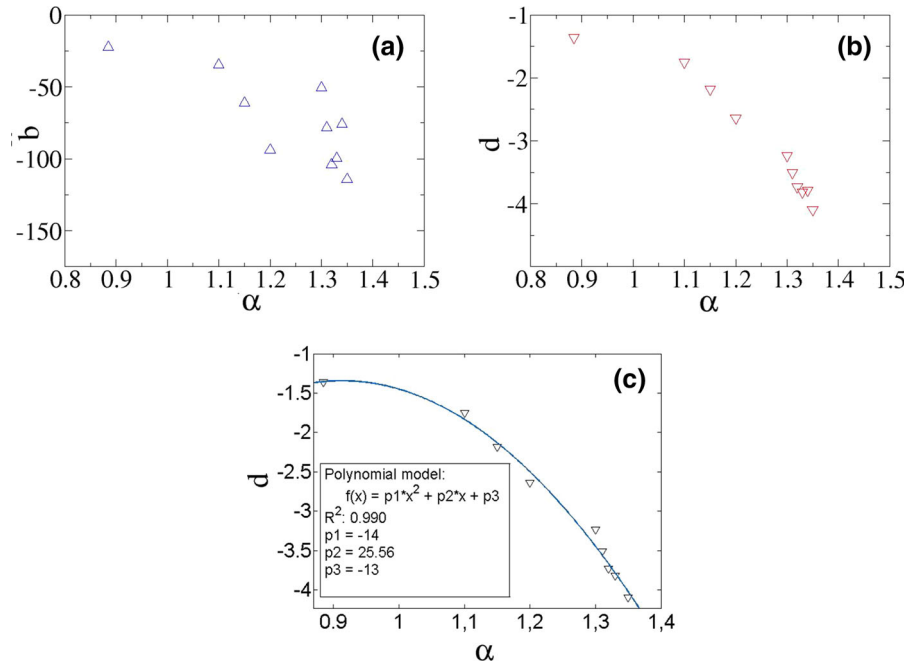


Fig. 10 **a** Average escape times from the well for $\alpha = 1.35$ and different initial conditions inside the well. **b** The same for $\alpha = 1.36$. It is possible to observe that from values of $\alpha \approx 1.36$ the escape times, before to show the monotonic decay, have fluctuations

to 1.36 (Fig. 10b). Through the figures analysis, we can determine that the appearance of the peaks (Fig. 10b), due to the fractalization of the attractor boundaries [20], inhibited us to keep going on to larger values of α then 1.36 for the study of the exponential parameter variation.

The plot of the exponential parameter b, d in function of the parameter α is shown in Fig. 11a–b, respectively. It is important to say that all the curves from which we have got those values of b and d show a $R^2 > 0.99$. Differently from the underdamped case, we can find here a common trend for the escape time distribution all along the attractor boundary, possibly an effect of the high damping parameter value. In Fig. 11a, we can observe some fluctuations for $0.8 < \alpha < 1.4$. However, in Fig. 11b, a nonlinear decrease in d versus α is observed. The corresponding terms of this decay law are shown in Fig. 11c. In that figure, a polynomial decay law fits the data very well since the regression coefficient $R^2 \approx 0.99$. Therefore, we can write the mathematical expression of this curve as follows:

Fig. 11 **a** and **b** show, respectively, the dynamics of the decay law exponentials (b , d), calculated as in figures 9 in function of the α values smaller than $\alpha = 1.36$, value for which the boundaries fluctuations of the escape times begin. **c** a regression curve for the dynamics of parameter d in function of the fractional derivative parameter α , shown in (**b**), is proposed



$$d(\alpha) = p_1\alpha^2 + p_2\alpha + p_3, \tag{7}$$

with $p_1 = -14$, $p_2 = 25.56$ and $p_3 = -13$.

The polynomial fitting of d versus α connects with the exponential fitting shown in Fig. 9 and in Fig. 12. For that reason, we can say that the two figures are related. In fact, the curves in Fig. 9b and in Fig. 12 cross each other in the following points: $t = 1.1$ for $x_0 = 0.5$ in the first one and for $\alpha = 1.3$ in the second one. Furthermore, the trend of the parameter d versus α is as we expected since the curve of the distribution of the escape time t in function of x_0 , reads:

$$t(x_0) = ae^{bx_0} + ce^{dx_0} \tag{8}$$

in which the first term is negligible because of the parameter values a , b . Therefore, the main term of the regression curve can be written as follows:

$$t(x_0) \approx ce^{dx_0}. \tag{9}$$

Finally, we substitute d as Eq. (7), for values of the initial condition $x_0 > 0$ obtaining an exponential decay law similar to the one shown in Fig. 12.

Finally, in the latter figure, the study of the average escape times, by varying α for a fixed value $x_0 = 0.5$, shows that the fractional damping term can be used

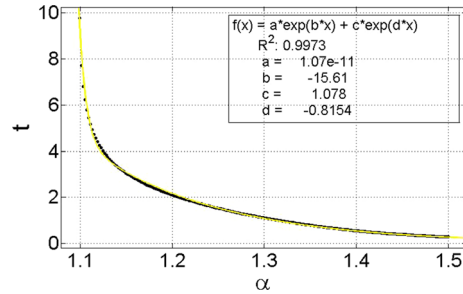


Fig. 12 Average escape times from the well for fixed $x_0 = 0.5$ and from the first α value for which the trajectories escape from the well, from $\alpha \approx 1.0995$ to 1.5

as a control parameter for the escape of the particles from the potential well. In this sense, when we move from points which are on the smooth boundaries of the attractor, the escape times of the particles decrease insofar the values of α are going far away from the attractor, as shown in Fig. 12. It can be seen that all of the escape times cases exposed are shown in Figs. 7 and 8.

Now, in order to follow the same path as in the under-damped case, we show the final state of the system in Fig. 13a, and the escape times gradient in Fig. 13b, in function of the simultaneous variations of F and α . In Fig. 13a, the parameter values for which the particles do not escape are colored in gray (yellow online) and

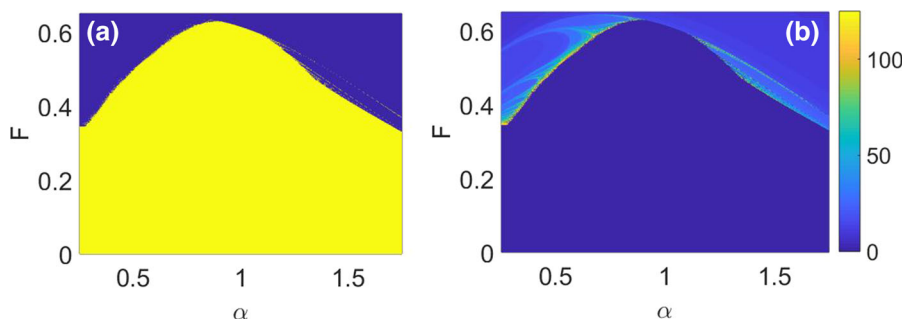
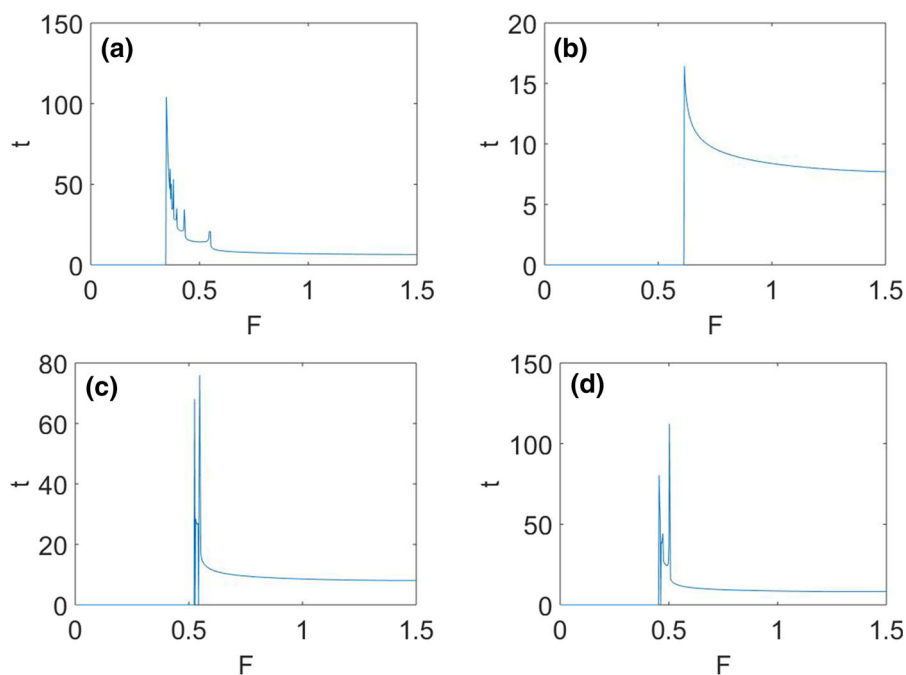


Fig. 13 **a** the panel shows the final state of the system taking $\alpha = [0.35, 1.5]$ and $F = [0, 0.7]$ and keeping constant the rest of the parameters. Gray color (yellow on line) implies the particle remains inside the potential well and black color (blue on

line) that particle escapes from it. **b** the panel shows, for the same range of F and α and the same parameter as in figure **(a)**, the gradient escape times. A semi parabolic shape denotes the behavior of the particle as α and F vary

Fig. 14 The panel shows the particle escape times from the potential well with $\alpha = 0.25, 1, 1.25, 1.39$, by reading the figures from **(a)** to **(d)**, and varying F

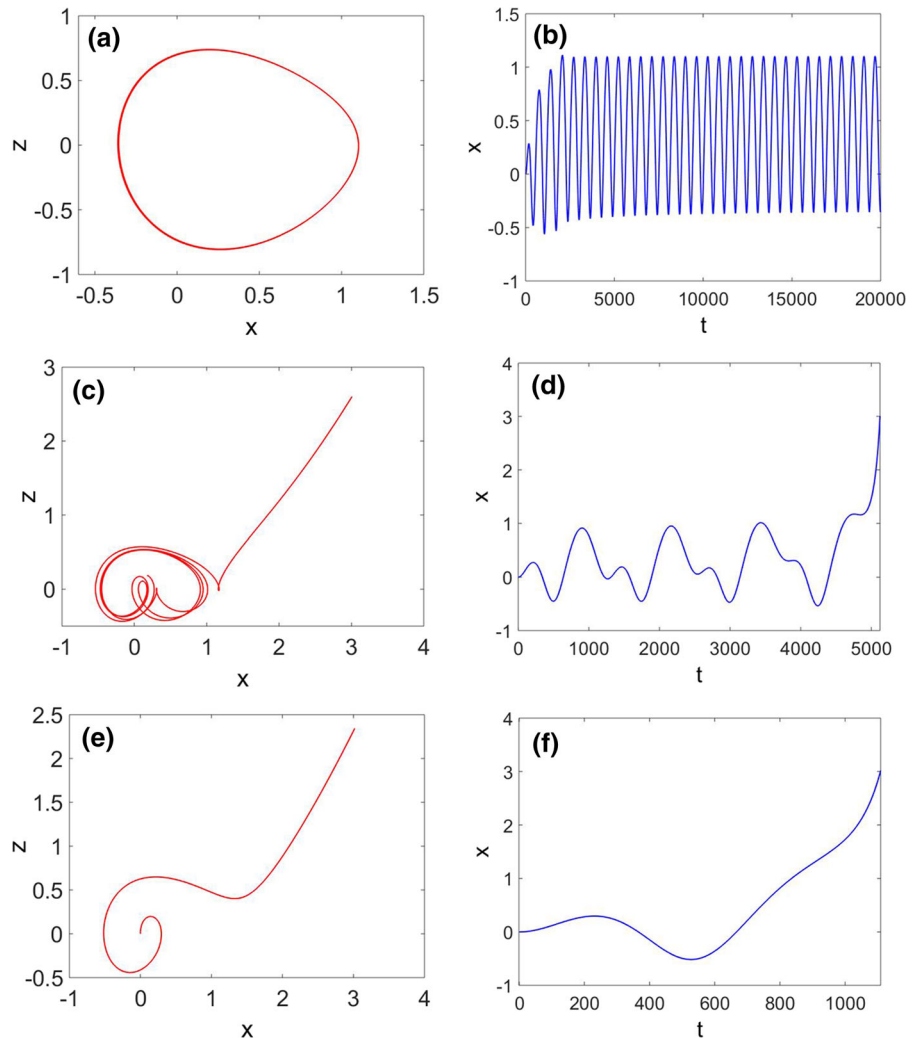


the black color (blue online) is used for the different case. It is interesting the semi parabolic shape in both Fig. 13a–b. Again, as shown in Fig. 13b, the closer the values of F and α are to the values on the boundaries for which there is no escape, the higher the time of the escape.

Then, we considered distributions of the escape times, t , in function of the periodic forcing F to study the behavior of the escape times from another point of view. Different results have been obtained and are shown in Fig. 14a–d. For the numerical simulations, we choose the values of $\alpha = 0.5, 1, 1.25, 1.39$, respec-

tively, and we vary F for the zero-initial conditions. Figure 14a represents the case when $\alpha = 0.25$. In this first plot we can see the fluctuations of the escape time for the first values in the interval, but from $F \approx 0.6$ we obtained a smooth curve due to the strong effect of the high values of F . In the next plot, we have repeated the same experiment with $\alpha = 1$ and we show the results in Fig. 14b. For this α values, differently from the underdamped case, the figure illustrates a whole smooth curve for every value of F and, as the fractalization is not present, very short escape times in comparison with Fig. 5d. This is a counterintuitive result,

Fig. 15 The panel shows the behavior of the fractional damping Helmholtz oscillator with different values of α at zero-initial conditions and $\mu = 0.8$, $F = 0.46$ and $\omega = 1$. **a**, **c** and **d** show the trajectories of Helmholtz oscillator x vs z , while figures **b**, **d** and **f** the oscillations of the position x with time, for $\alpha = 0.5$, $\alpha = 1.39$, $\alpha = 1.75$, respectively. **a** and **b** represents the typical bounded orbit inside the potential well. **c** and **d** plot the trajectory that escape the potential well. The last figures plot a trajectory with a shorter escape time

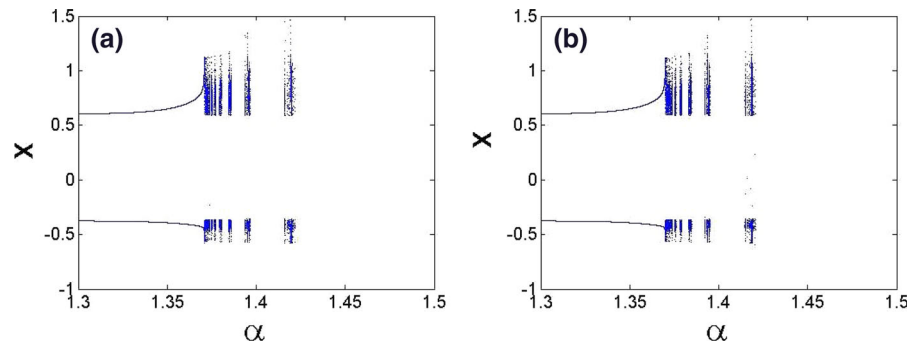


as we have commented along the paper, the higher the dissipation the longer the escape times. Here, on the other hand, the escape times diminish in the over-damped case, since the higher value of the damping term makes the boundaries of the attractors smooth and so the escape times become smaller. This is a different behavior, compared with the above case, $\alpha = 0.25$. This shows that the fractalization induced by the fractional term has a deep impact on the dynamics of the system. The next experiments with $\alpha = 1.25$, 1.39 , are respectively shown in Fig. 14c–d. The trend of these two cases is similar. Again, we obtained fluctuations in the escape times for the first values of F and near $F = 0.6$ the curves become smooth. Therefore, as we already know from Fig. 13, the first value of F for which the particle escape depend on the value of α , and the

dependence is not linear. As it happened in the under-damped case, the fluctuations, due to the fractalization of the boundaries, impede us to study a general decay law for the escape times as we did for the $\{\alpha - x_0\}$ plane, where a smooth boundary was present. All this analysis suggests that the variation of the parameter α along with the forcing amplitude F can be responsible of deep changes in the dynamics of the system, due to the induction of the fractalization of the parameter space. This means that α is a suitable control parameter for the behavior of the system.

In order to have a better understanding of the dynamics of the system, we plot the trajectories with different values of the α parameter in Fig. 15 by fixing the value of the damping $\mu = 0.8$, the forcing amplitude $F = 0.46$, the frequency $\omega = 1$ and the zero-initial conditions.

Fig. 16 Bifurcation diagram with $x_0 = 0.0$, $\mu = 0.8$, $F = 0.46$ and $\omega = 1$ (a). Bifurcation diagram with $x_0 = 0.01$, $\mu = 0.8$, $F = 0.46$ and $\omega = 1$ (b)



In Fig. 15a–b we take $\alpha = 0.5$ and we can see the closed orbit and the evolution with time of the trajectory described by the system. Next case we consider is $\alpha = 1.39$ which is depicted in Fig. 15c, d. This value of α generates escapes from the potential well even considering zero-initial conditions. This abrupt change in the dynamics is an interesting issue that reveals, again, the dependence on the fractional damping term. Another important fact is that this result confirms the importance to study the effect of taking a specific value of α and measure the escape times depending on different initial conditions. Thus, Fig. 15c shows that the trajectory is initially contained in the well but at certain time it escapes from it. In fact, in Fig. 15d, we show the escaping from the potential well other than the oscillations before. We also consider the case of $\alpha = 1.75$ another case for which the trajectory is escaping from the well, according to the numerical results shown in Figs. 15e and 11f. The difference is that for this value of α the oscillator behaviors before the escape die out faster than the case for $\alpha = 1.39$. So that, indeed α can be considered as a control parameter of the system, which confirms its relevance in this work.

Now, to stress out this crucial role of the α parameter, in the overdamped case, we have considered important to analyze the dynamics of the system in function of the α variation with a bifurcation diagram, see Fig. 16a–b. These figures show two different bifurcation diagrams with just a little difference on their initial conditions. In both figures the dynamics related with escapes have been left white, for an easier reading of the graphics. Figure 16a corresponds to initial conditions $(x_0, y_0, z_0) = (0, 0, 0)$ and α has been considered from 1.3 to 1.5. Figure 16b has been drawn with a slightly different initial conditions, $(x_0, y_0, z_0) = (0.01, 0, 0)$. The figures show the effectiveness of α as a control parameter. In fact, the results, that match with the pre-

vious ones of Figs. 7 and 8, confirm that the α parameter can induce chaos in the system, even in the overdamped case, and that its appearance is robust for small variation of the initial conditions.

5 Conclusions

We have studied, using the Grünwald–Letnikov integrator, the dynamics of the fractional Helmholtz oscillator with fractional term in the underdamped and the overdamped cases. Since the system allows the particle to escape the potential well, we used the attractor and the escape time plots as tools to analyze the impact of the fractional parameter on the dynamics of the system. In the underdamped case, the dynamics of the system are already rich and all kind of behavior are possible. However, changing the fractional parameter has a big impact on the system dynamics. On the other hand, the second case that is normally not so interesting because the high dissipation makes the system more predictable, becomes more interesting when the fractional derivative is introduced. In fact, in the overdamped case is where the crucial role of the fractional parameter becomes evident. When we vary the initial conditions and the fractional parameter, all kind of behavior of the system are possible, even chaotic. All this variety of the system dynamics appears, in the attractor and escape time gradient plots, as a fractalization of the parameter space in function of the variation of the fractional parameter. All this makes the fractional parameter a suitable candidate to control the asymptotic behaviors of the system. Moreover, in both cases, the escape time plots showed us that near the boundaries of the attractor they are higher. However, in the overdamped case, the escape time distribution of the particles show an exponential-like decay law.

Finally, in the overdamped case we have studied the bifurcation diagrams in function of α to contrast the previous results. Also, we have seen that the appearance of chaotic behavior is robust for small changes, inside certain interval, of the initial condition, and the α parameter.

To summarize, chaotic and periodic regions appearance in the parameter space depends on the fractional parameter. So that we can say that it acts as a control parameter of the dynamics of the Helmholtz oscillator. In fact, the computation of the basins of the final state and the gradient of the escape times of our model in the parameter space corroborates the previous conclusions. We expect these results to be useful for a better understanding of fractional calculus in chaotic systems since the memory effects are relevant on their dynamics.

Acknowledgements This work has been supported by the Spanish State Research Agency (AEI) and the European Regional Development Fund (ERDF, EU) under Projects No. FIS2016-76883-P and No. PID2019-105554GB-I00, and the National Natural Science Foundation of China (Grant No. 11672325).

Compliance with ethical standards

Conflict of interest: The authors declare that they have no conflict of interest.

References

1. Yang, X.: General Fractional Derivatives: Theory, Methods and Applications. CRC Press, New York (2019)
2. Wang, Z., Huang, X., Zhao, Z.: Synchronization of nonidentical chaotic fractional-order systems with different orders of fractional derivatives. *Nonlinear Dyn.* **69**, 999–1007 (2012)
3. Ezz-Eldien, S.S., Doha, E.H., Baleanu, D., Bhrawy, A.H.: A numerical approach based on Legendre orthonormal polynomials for numerical solutions of fractional optimal control problems. *J. Vib. Control* **23**, 16–30 (2017)
4. Baleanu, D., Wu, G.C., Bai, Y.R., Chen, F.L.: Stability analysis of Caputo-like discrete fractional systems. *Commun. Nonlinear Sci. Numer. Simulat.* **48**, 520–530 (2017)
5. Yang, X.J., Gao, F., Srivastava, H.M.: New rheological models within local fractional derivative. *Rom. Rep. Phys.* **69**(3), 113 (2017)
6. Khennaoui, A., Ouannas, A., Bendoukha, S., Grassi, G., Pierre Lozi, R., Pham, V.: On fractional-order discrete-time systems: Chaos, stabilization and synchronization. *Chaos Solitons Fractals* **119**, 150–162 (2019)
7. Zhang, S., Liu, L., Xue, D., Chen, Y.: Stability and resonance analysis of a general non-commensurate elementary fractional-order system. *Fract. Calc. Appl. Anal.* **23**, 183–210 (2020)
8. He, J.H., Ji, F.Y.: Two-scale mathematics and fractional calculus for thermodynamics. *Thermal Sci.* **23**, 2131–2133 (2019)
9. Ionescu, C., Lopes, A., Copot, D., Machado, J.T., Bates, J.H.T.: The role of fractional calculus in modeling biological phenomena: a review. *Commun. Nonlinear Sci. Numer. Simulat.* **51**, 141–159 (2017)
10. Niu, J., Liu, R., Shen, Y., Yang, S.: Chaos detection of Duffing system with fractional-order derivative by Melnikov method. *Chaos* **29**, 123106 (2019)
11. He, S., Sun, K., Peng, Y.: Detecting chaos in fractional-order nonlinear systems using the smaller alignment index. *Phys. Lett. A* **383**, 2267–2271 (2019)
12. Jiménez, S., González, J.A., Vázquez, L.: Fractional Duffing's equation and geometrical resonance. *Int. J. Bifurc. Chaos* **23**, 1–13 (2013)
13. Sun, H., Zhang, Y., Baleanu, D., Chen, W., Chen, Y.: A new collection of real world applications of fractional calculus in science and engineering. *Commun. Nonlinear Sci. Numer. Simulat.* **64**, 213–231 (2018)
14. Velasco, M.P., Usero, D., Jiménez, S., Vázquez, L., Vázquez-Poletti, J.L., Mortazavi, M.: About some possible implementations of the fractional calculus. *Mathematics* **8**, 893 (2020)
15. Yang, X.J., Baleanu, D., Gao, F.: New analytical solutions for Klein–Gordon and Helmholtz equations in fractal dimensional space. *Proc. Rom. Acad., Ser. A: Math. Phys. Tech. Sci. Inf. Sci.* **18**, 231–238 (2017)
16. Ouannas, A., Almatroud, O.A., Khennaoui, A.A., Alsawalha, M.M., Baleanu, D., Huynh, V.V., Pham, V.-T.: Bifurcations, hidden chaos and control in fractional maps. *Symmetry* **12**, 879 (2020)
17. Wang, Z., Shiri, B., Baleanu, D.: Discrete fractional watermark technique. *Front. Inform. Technol. Electron. Eng.* **21**, 880–883 (2020)
18. Atangana, A., Gómez-Aguilar, J.F.: Decolonisation of fractional calculus rules: breaking commutativity and associativity to capture more natural phenomena. *Eur. Phys. J. Plus* **133**, 1–23 (2018)
19. Diethelm, K., Ford, N.J., Freed, A.D., Luchko, Y.: Algorithms for the fractional calculus: a selection of numerical methods. *Comput. Methods Appl. Mech. Eng.* **194**, 743–773 (2005)
20. Scherer, R., Kalla, S.L., Tang, Y., Huang, J.: The Grünwald-Letnikov method for fractional differential equations. *Comput. Math. Appl.* **62**, 902–917 (2011)
21. Seoane, J.M., Zambrano, S., Euzzor, S., Meucci, R., Arecchi, F.T., Sanjuán, M.A.F.: Avoiding escapes in open dynamical systems using phase control. *Phys. Rev. E* **78**, 1–8 (2008)

Publisher's Note Springer Nature remains neutral with regard to jurisdictional claims in published maps and institutional affiliations.